Journal of Science and Transport Technology
Journal homepage: https://jstt.vn/index.php/en

Thermo-Mechanical Post-Buckling Analysis of 3D Graphene Foam Shallow Spherical Shells and Circular Plates Stiffened by a Spider-Web Stiffener System: A Stress Function Approach

Article info
Type of article:
Original research paper

DOI:
https://doi.org/10.58845/jstt.utt.2026.en.6.2.132-149

***Corresponding author:**
Email address:
thanhhoai.nguyen@utc.edu.vn

Received: 21/09/2025
Received in Revised Form: 24/11/2025
Accepted: 19/12/2025

Dang Thuy Dong[1,2], Nguyen Thi Thanh Hoai[3,4*], Doan Lan Phuong[5]
[1]Mechanics of Advanced Materials and Structures, Institute for Advanced Study in Technology, Ton Duc Thang University, Ho Chi Minh City, Vietnam
[2]Faculty of Civil Engineering, Ton Duc Thang University, Ho Chi Minh City, Vietnam
[3]Faculty of International Education, University of Transport and Communications, Hanoi, Vietnam
[4]Graduate University of Science and Technology, Vietnam Academy of Science and Technology, Hanoi, Vietnam
[5]Mechanics of Advanced Materials and Structures, University of Transport Technology, Hanoi, Vietnam

Abstract: This study focuses on analyzing the nonlinear post-buckling response of shallow spherical shells and circular plates resting on a nonlinear elastic foundation and subjected to combined mechanical and thermal loads. The spherical shell or circular plate is made of 3D graphene foam material and is stiffened by a spider-web stiffener system, which is also composed of 3D graphene foam. The fundamental formulations and governing equations are derived based on Donnell's shell theory, incorporating von Kármán geometric nonlinearity. The stiffness components of the stiffened plate/shell structures are determined using the extended stiffener-smearing technique. By employing the stress function approach and the Ritz energy method, analytical expressions for the load-deflection relationship are obtained. Numerical examples are then carried out to investigate the post-buckling behavior of the stiffened shallow spherical shells and circular plates under the influence of material, geometric, and foundation parameters.

Keywords: Thermo-Mechanical Post-Buckling, 3D graphene foam, Spiderweb stiffener, Spherical shell, Circular plate.

1. Introduction

Circular plates (CiPls) and shallow spherical shells (SSpShs) are widely used in various scientific and engineering fields. Their geometric symmetry enables uniform stress distribution and provides excellent resistance to buckling, making them suitable for applications such as dome roofs, radar covers, pressure vessels in spacecraft, and fuel tank caps [1-3]. The static and dynamic behaviors of SSpShs and CiPls have been extensively investigated by numerous researchers worldwide. Among the earliest works, Kalnins and

Naghdi [4], Grossman et al. [5], and Sathyamoorthy [6] focused on the vibration analysis of isotropic SSpShs based on various models and theories. The stability of SSpSh with dynamic boundary conditions accounting for line tension was analyzed by Abels et al. [7]. The nonlinear axisymmetric bending analysis of CiPls was investigated by Li et al. [8] using the strain-gradient theory and differential quadrature method. By using the first-order shear deformation theory (FSDT), the dynamic and static behavior of hyperelastic CiPls was studied by Najafipour and Shariyat [9] under pressurized and blasted loads.

The functionally graded material (FGM) SSpShs and CiPls have been studied using different analytical and numerical methods. By employing the FSDT and Ritz method, Kiani [10] studied the static and dynamic snap-through buckling responses of FGM CiPls. Ahmadi and Foroutan [11] investigated the nonlinear dynamic buckling responses of porous FGM SSpShs. Based on the Timoshenko-Mindlin hypothesis, Fu et al. [12] investigated the transient deformation of FGM SSpShs. By applying the Galerkin method and FSDT, Anh and Duc [13] analyzed the nonlinear thermo-mechanical stability of thick S-FGM SSpShs, Phuong et al. [14] studied the nonlinear forced vibration problem of the sandwich FGM SSpShs. Zhou et al. [15] studied the axisymmetric vibration behavior of the FG piezoelectric CiPls by applying the quadrature-free method. The HSDT and Ritz method were also used by Ly et al. [16] to analyze the nonlinear buckling behavior of sandwich FG SSpShs. Various boundary conditions were investigated, and the nonlinear thermally shocked responses of FG SSpShs were analyzed by applying the DQM and Newmark procedure [17].

Recently, a new advanced composite material, namely functionally graded graphene-platelet-reinforced composite (FG-GPLRC), has shown great potential in applications. The linear buckling behavior of FG-GPLRC CiPls was investigated by Chien and Phuc [18] using HSDT and moving Kriging meshfree method. Liu et al. [19] studied the linear and nonlinear free vibration problems of FG-GPLRC SSpShs and CiPls using 3D elasticity theory. Chu et al. [20] and Javani et al. [21] considered nonlinear vibration and dynamic stability responses of the FG-GPLRC CiPls using Donnell shell theory, FSDT, and HSDT, respectively. By using the energy method and displacement approach, Tu et al. [22] investigated the nonlinear dynamic thermo-mechanical buckling and vibration of FG-GPLRC CiPls and SSpShs. The stability and post-buckling responses of FG-GPLRC SSpShs, and FG-GPLRC SSpShs with a porous core, were separately investigated by Phuong et al. [23] and Ly et al. [24]. Their studies employed HSDT and the Ritz energy method. Porosities are introduced into the FG-GPLRC through various distribution laws, forming a new composite known as 3D graphene foam. This material integrates the superior in-plane stiffness of graphene with ultralight porous scaffolds, resulting in high specific stiffness, excellent thermal conductivity, and promising applications in energy absorption, heat dissipation, and lightweight reinforcement [25, 26].

Khatounabadi and Jafari [27] presented the low-velocity impact analysis of 3D graphene foam CiPls based on FSDT and Hamilton's principle. Using the Galerkin method, Tu et al. [28] investigated nonlinear buckling and post-buckling behavior of 3D graphene foam shallow complex curved caps and CiPls.

The addition of stiffeners offers an efficient way to enhance the strength of shells and plates. The smeared stiffener method, developed initially by Lekhnitskii [29] and later extended by Jaunky et al. [30], has become a cornerstone of analytical stiffened panel design. The use of stiffeners for plate/shell structures has been shown to have many outstanding advantages [31, 32].

Studies on the nonlinear stability and dynamics of plates and shells reinforced by

stiffener systems with variable mechanical properties of nanocomposite materials have been carried out by Nam et al. [33-36]. The application of stiffener systems to SSpShs presents difficulties due to the non-uniform spacing between adjacent radial stiffeners. Consequently, the implementation of Lekhnitskii's classical homogenization technique for stiffener action becomes challenging. By expanding Lekhnitskii's smeared stiffener technique and employing the Ritz energy method, Nam et al. [36] presented a new analytical approach for the static stability problems of SSpShs and CiPls reinforced by spiderweb stiffeners.

In addition, the common point of most previous studies on the mechanical behavior of SSpShs and CiPls is to use the displacement approach to solve the problem. In contrast, employing the stress-function approach naturally satisfies the equilibrium conditions and significantly reduces the number of governing equations. This provides a more compact and efficient framework for analyzing the nonlinear buckling and post-buckling behavior of the structures. Therefore, in this study, a new stress-function approach is used to analyze the nonlinear stability of stiffened 3D graphene foam SSpShs and CiPls subjected to thermal-mechanical loads. The basic formulas and equations are established based on the Donnell thin-shell theory and von Kármán's geometric nonlinearity. By using the stress-function approach combined with the Ritz energy method, the load-deflection relationships are obtained. The effects of 3D graphene foam, stiffeners, and geometric parameters on nonlinear post-buckling responses are investigated.

2. Configuration and material properties of stiffened 3D graphene foam SSpSh

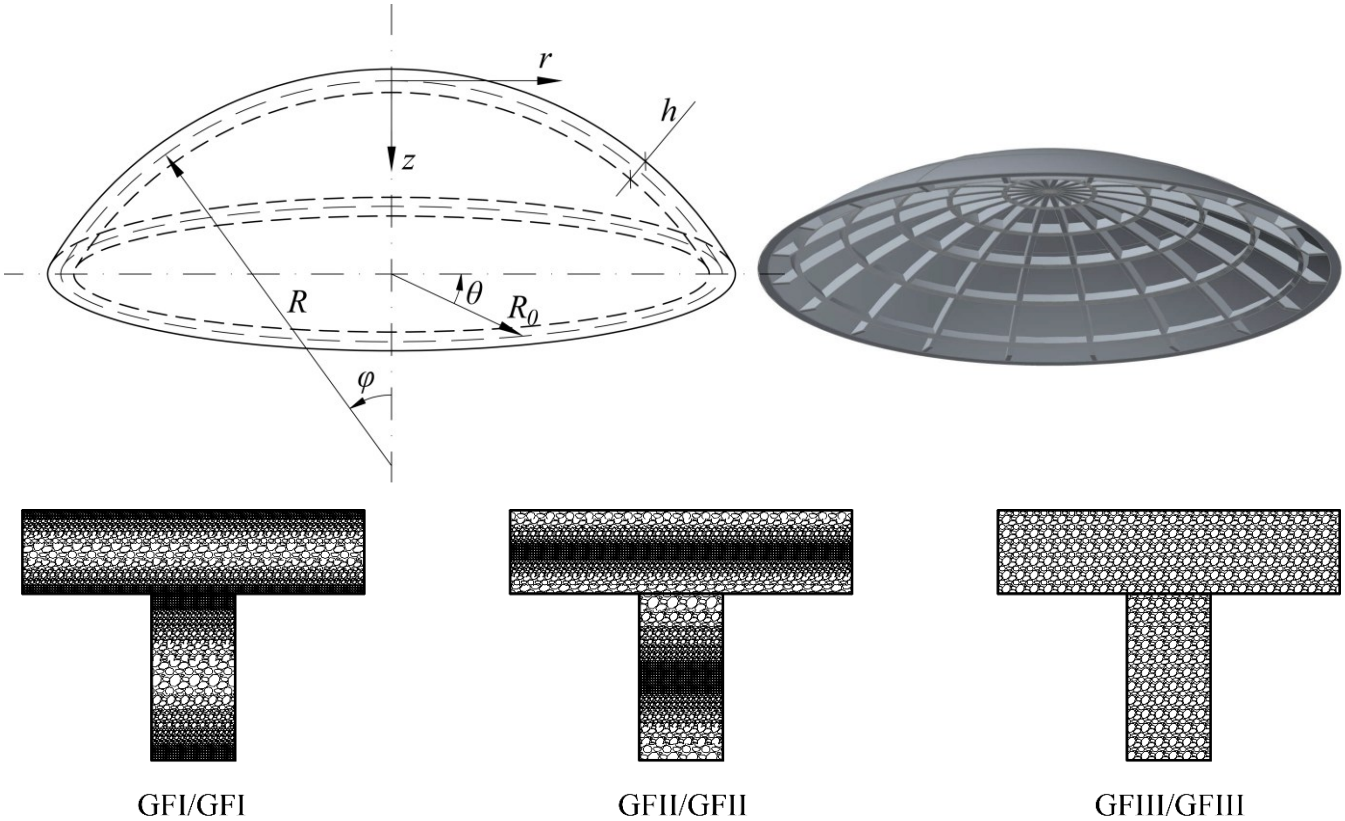

Fig. 1. Configuration, coordinate system, and material distributions of SSpSh and stiffeners

An axisymmetric deformable SSpShs made from 3D graphene foam, resting on a Pasternak elastic foundation, is shown in Fig. 1. This shell has the thickness h, a radius of shell curvature R and base radius R_0. The SSpSh is under the time-dependent external pressure load q, which is

uniformly distributed on the inner surface of the structure. The SSpSh is defined in the coordinate system (φ,θ,z), where φ and θ denote the radial and circumferential directions, respectively, and z is the concentric coordinate. The radius of the parallel of latitude can be defined as $r=R\sin\varphi$. According to the shallow shell assumption of the SSpSh, the approximations $\cos\varphi\approx 1$ and $Rd\varphi\approx dr$ can be used to introduce the simpler coordinate system (r,θ,z) as illustrated in Fig. 1. A radial and circumferential spiderweb stiffener system is used to reinforce the SSpSh.

Note that the governing equations are established for the SSpShs, and those of the CiPls are determined by approaching the main radius of curvature to infinity $R\to\infty$.

The 3D graphene foam spherical shells resting on the nonlinear elastic foundation are considered to be axisymmetrically deformed. The shells are subjected to external pressure loads q and/or thermal loads ΔT. The shells are stiffened by radial and circumferential 3D graphene foam stiffeners. As illustrated in Fig. 1, the shells are placed in the (φ,θ,z) coordinate system, and the simpler quasi-polar coordinate system (r,θ,z) is introduced.

The 3D graphene foam is used to make both the shell skin and spiderweb stiffeners. To ensure material continuity for the shell skin and stiffeners, three shell/stiffener material distribution patterns were considered, respectively: GFI/GFI, GFII/GFII, GFIII/GFIII, as shown in Fig. 1.

The effective properties of the 3D graphene foam shell and stiffeners are assumed to be in the following forms [37]:

- For the shell $(-h/2\le z\le h/2)$

$$E_{GF}^{sh}(z)=\begin{cases}E_h\left[1-e_{1h}\delta_{1h}(z)\right] & \text{GFI}\\ E_h\left\{1-e_{2h}\left[1-\delta_{1h}(z)\right]\right\} & \text{GFII}\\ E_h e_{3h} & \text{GFIII}\end{cases} \quad (1)$$

$$\nu_{GF}^{sh}(z)=\nu_h,\ \alpha_{GF}^{sh}(z)=\alpha_h, \quad (2)$$

$$\rho_{GF}^{sh}(z)=\begin{cases}\rho_h\left[1-\bar{e}_{1h}\delta_{1h}(z)\right] & \text{GFI}\\ \rho_h\left\{1-\bar{e}_{2h}\left[1-\delta_{1h}(z)\right]\right\} & \text{GFII}\\ \rho_h\bar{e}_{3h} & \text{GFIII}\end{cases} \quad (3)$$

- For the stiffeners $(h/2\le z\le h/2+h_{st})$

$$E_{GF}^{st}(z)=\begin{cases}E_{h_{st}}\left[1-e_{1h_{st}}\delta_{1h_{st}}(z)\right] & \text{GFI}\\ E_{h_{st}}\left\{1-e_{2h_{st}}\left[1-\delta_{1h_{st}}(z)\right]\right\} & \text{GFII}\\ E_{h_{st}}e_{3h_{st}} & \text{GFIII}\end{cases} \quad (4)$$

$$\rho_{GF}^{st}(z)=\begin{cases}\rho_{h_{st}}\left[1-\bar{e}_{1h_{st}}\delta_{1h_{st}}(z)\right] & \text{GFI}\\ \rho_{h_{st}}\left\{1-\bar{e}_{2h_{st}}\left[1-\delta_{1h_{st}}(z)\right]\right\} & \text{GFII}\\ \rho_{h_{st}}\bar{e}_{3h_{st}} & \text{GFIII}\end{cases} \quad (5)$$

$$\nu_{GF}^{h_{st}}(z)=\nu_{h_{st}},\ \alpha_{GF}^{h_{st}}(z)=\alpha_{h_{st}}, \quad (6)$$

with $\delta_{1h_{st}}(z)=\cos\left(\dfrac{\pi(2z-h-h_{st})}{2h_{st}}\right)$,

$\delta_{1h}(z)=\cos\left(\dfrac{\pi z}{h}\right)$; e_{jh}, $e_{jh_{st}}$ and $\bar{e}_{jh}$, $\bar{e}_{jh_{st}}$ (j=1, 2, 3) are the porosity coefficients and mass density coefficients, respectively; h and h_{st} are the SSpSh thickness and height of stiffeners, respectively, ρ_k, E_k, ν_k, and α_k $(k=h,h_{st})$ are the mass density, elastic modulus, Poisson's ratio, and thermal expansion coefficients of the shell (for $k=h$) and the stiffeners (for $k=h_{st}$) without porosities, respectively.

According to the extended Halpin-Tsai model, the predicted elastic modulus of FG-GPLRC is calculated by [37]

- For the shell

$$E_{sh}(z)=\frac{E_M}{8}\times\left\{\frac{3\left[1+a_1b_1V_{GPLsh}(z)\right]}{1-b_1V_{GPLsh}(z)}+\frac{5\left[1+a_2b_2V_{GPLsh}(z)\right]}{1-b_2V_{GPLsh}(z)}\right\}, \quad (7)$$

- For the stiffeners

$$E_{st}(z)=\frac{E_M}{8}\times \left\{\frac{3\left[1+a_1b_1V_{GPLst}(z)\right]}{1-b_1V_{GPLst}(z)}+\frac{5\left[1+a_2b_2V_{GPLst}(z)\right]}{1-b_2V_{GPLst}(z)}\right\}, \quad (8)$$

where E_M is the elastic modulus of the matrix, and

$$a_1=2(\gamma_{GPL}/h_{GPL}),\ a_2=2(\lambda_{GPL}/h_{GPL}),$$
$$b_1=\left[(E_{GPL}/E_M)-1\right]/\left[(E_{GPL}/E_M)+a_1\right], \quad (9)$$
$$b_2=\left[(E_{GPL}/E_M)-1\right]/\left[(E_{GPL}/E_M)+a_2\right],$$

where γ_{GPL}, λ_{GPL} and h_{GPL} are the length, width, and thickness of the GPL; and E_{GPL} is the elastic modulus of the GPLs.

The effective thermal expansion coefficient and Poisson ratio are determined using the mixed rule, as follows

- For the shell

$$\alpha_{sh}(z)=\alpha_M(1-V_{GPLsh})+\alpha_{GPL}V_{GPLsh},$$
$$\nu_{sh}(z)=\nu_M(1-V_{GPLsh})+\nu_{GPL}V_{GPLsh}, \quad (10)$$

- For the stiffeners

$$\alpha_{st}(z)=\alpha_M(1-V_{GPLst})+\alpha_{GPL}V_{GPLst},$$
$$\nu_{st}(z)=\nu_M(1-V_{GPLst})+\nu_{GPL}V_{GPLst}, \quad (11)$$

where α_M, α_{GPL} and ν_M, ν_{GPL} are the thermal expansion coefficient and Poisson ratio of the matrix and GPL, respectively.

The GPL volume fractions V_{GPLsh} and V_{GPLst} of the GPLRC shell and stiffeners are estimated, respectively, by

$$V_{GPLsh}=\rho_M\frac{W_{GPLsh}}{\rho_{GPL}(1-W_{GPLsh})+\rho_MW_{GPLsh}}, \quad (12)$$

$$V_{GPLst}=\rho_M\frac{W_{GPLst}}{\rho_{GPL}(1-W_{GPLst})+\rho_MW_{GPLst}}, \quad (13)$$

with W_{GPLsh} and W_{GPLst} are the mass fraction of GPLs in the SSpSh and the stiffeners; and ρ_M and ρ_{GPL} are the mass densities of the matrix and the GPL, respectively.

The relations between the elastic modulus and mass density of 3D graphene foam and GPLRC in the shell skin and the stiffeners are presented for a spherical shell [37], as

$$\frac{E_{GF}^{sh}}{E_h}=\left[\frac{\rho_{GF}^{sh}}{\rho_h}\right]^2. \quad (14)$$

and for stiffeners

$$\frac{E_{GF}^{st}}{E_{h_{st}}}=\left[\frac{\rho_{GF}^{st}}{\rho_{h_{st}}}\right]^2. \quad (15)$$

The relations between the foam coefficients and the mass density coefficients of the GPLRC in the shell skin and the stiffeners are obtained by employing the relations (14) and (15), taking into account Eqs. (1), (2), (4), and (5) for the SSpSh ($-h/2\le z\le h/2$)

$$\begin{cases}1-\bar{e}_{1h}\delta_{1h}(z)=\sqrt{1-e_{1h}\delta_{1h}(z)} & \text{GFI}\\ 1-\bar{e}_{2h}\left[1-\delta_{1h}(z)\right]=\sqrt{1-e_{2h}\left[1-\delta_{1h}(z)\right]} & \text{GFII}\\ \bar{e}_{3h}=\sqrt{e_{3h}} & \text{GFIII}\end{cases} \quad (16)$$

and for the stiffeners ($h/2\le z\le h/2+h_{st}/2$)

$$\begin{cases}1-\bar{e}_{1h_{st}}\delta_{1h}(z)=\sqrt{1-e_{1h_{st}}\delta_{1h_{st}}(z)} & \text{GFI}\\ 1-\bar{e}_{2h_{st}}\left[1-\delta_{1h_{st}}(z)\right]=\sqrt{1-e_{2h_{st}}\left[1-\delta_{1h_{st}}(z)\right]} & \text{GFII}\\ \bar{e}_{3h_{st}}=\sqrt{e_{3h_{st}}} & \text{GFIII}\end{cases} \quad (17)$$

The mass of the matrix is considered to be constant with different foam distributions. From Eqs. (16) and (17), the following relations are obtained for the shells ($-h/2\le z\le h/2$)

$$\int_0^{h/2}\sqrt{1-e_{1h}\delta_{1h}(z)}dz=\int_0^{h/2}\sqrt{1-e_{2h}\left[1-\delta_{1h}(z)\right]}dz=\int_0^{h/2}\sqrt{e_{3h}}dz, \quad (18)$$

and for the stiffener ($h/2\le z\le h/2+h_{st}/2$)

$$\int_{h/2}^{h/2+h_{st}}\sqrt{1-e_{1hst}\delta_{1h}(z)}dz=\int_{h/2}^{h/2+h_{st}}\sqrt{1-e_{2h_{st}}\left[1-\delta_{1h}(z)\right]}dz=\int_{h/2}^{h/2+h_{st}}\sqrt{e_{3h_{st}}}dz, \quad (19)$$

where e_{2h}, e_{3h} and $e_{2h_{st}}, e_{3h_{st}}$ can be derived from the given values of e_{1h} and $e_{1h_{st}}$.

3. Fundamental formulations and energy method

According to the Donnell shell theory, the strain expressions are expressed by [36]

$$\begin{Bmatrix}\varepsilon_r\\ \varepsilon_\theta\end{Bmatrix}=\begin{Bmatrix}\varepsilon_{0r}\\ \varepsilon_{0\theta}\end{Bmatrix}-z\begin{Bmatrix}w_{,rr}\\ \dfrac{w_{,r}}{r}\end{Bmatrix}, \tag{20a}$$

$$\begin{Bmatrix}\varepsilon_{0r}\\ \varepsilon_{0\theta}\end{Bmatrix}=\begin{Bmatrix}u_{,r}-\dfrac{w}{R}+\dfrac{w_{,r}^2}{2}+w_{,r}\,w_{0,r}\\ \dfrac{u}{r}-\dfrac{w}{R}\end{Bmatrix}, \tag{20b}$$

where w_0 is the imperfect deflection.

By considering the thermal strains, the stress-strain relations are expressed as follows:

$$\begin{Bmatrix}\sigma_r\\ \sigma_\theta\end{Bmatrix}=\begin{bmatrix}Q_{11} & Q_{12}\\ Q_{12} & Q_{22}\end{bmatrix}\begin{bmatrix}\varepsilon_r-\alpha(z)\Delta T\\ \varepsilon_\theta-\alpha(z)\Delta T\end{bmatrix}. \tag{21}$$

The internal forces and moments are determined by

$$\begin{aligned}(N_r,M_r)&=\int_{-h/2}^{h/2}(1,z)\sigma_r dz,\\ (N_\theta,M_\theta)&=\int_{-h/2}^{h/2}(1,z)\sigma_\theta dz.\end{aligned} \tag{22}$$

By applying the extended smeared stiffener technique for spideweb 3D graphene foam stiffeners, as explained in detail in Ref. [36], the force and moment resultants are derived from expression (22) as follows

$$\begin{Bmatrix}N_r\\ N_\theta\\ M_r\\ M_\theta\end{Bmatrix}=\begin{Bmatrix}A_{11} & A_{12} & B_{11} & B_{12}\\ A_{12} & A_{22} & B_{12} & B_{22}\\ B_{11} & B_{12} & D_{11} & D_{12}\\ B_{12} & B_{22} & D_{12} & D_{22}\end{Bmatrix}\begin{Bmatrix}\varepsilon_{0r}\\ \varepsilon_{0\theta}\\ -w_{,rr}\\ -w_{,r}/r\end{Bmatrix}-\begin{Bmatrix}\Phi_{1r}\\ \Phi_{1\theta}\\ \Phi_{2r}\\ \Phi_{2\theta}\end{Bmatrix}\Delta T, \tag{23}$$

where $A_{ij},B_{ij},D_{ij}(ij=11,12,22)$ are the stiffnesses of stiffened SSpSh, expressed by

$$\begin{pmatrix}A_{11}\\ B_{11}\\ D_{11}\end{pmatrix}=\begin{pmatrix}A_{11}^{sh}+A_{11-in}^{st-m}+A_{11-ex}^{st-m}\\ B_{11}^{sh}+B_{11-in}^{st-m}+B_{11-ex}^{st-m}\\ D_{11}^{sh}+D_{11-in}^{st-m}+D_{11-ex}^{st-m}\end{pmatrix},$$

$$\begin{pmatrix}A_{22}\\ B_{22}\\ D_{22}\end{pmatrix}=\begin{pmatrix}A_{22}^{sh}+A_{22-in}^{st-m}+A_{22-ex}^{st-p}\\ B_{22}^{sh}+B_{22-in}^{st-m}+B_{22-ex}^{st-p}\\ D_{22}^{sh}+D_{22-in}^{st-m}+D_{22-ex}^{st-p}\end{pmatrix},$$

$$\begin{pmatrix}A_{12}\\ B_{12}\\ D_{12}\end{pmatrix}=\begin{pmatrix}A_{12}^{sh}+A_{12-in}^{st-m}\\ B_{12}^{sh}+B_{12-in}^{st-m}\\ D_{12}^{sh}+D_{12-in}^{st-m}\end{pmatrix},$$

$$\left(A_{ij}^{sh},B_{ij}^{sh},D_{ij}^{sh}\right)=\int_{-h/2}^{h/2}\left(1,z,z^2\right)Q_{ij}^{sh}dz,$$

$$\left(A_{ij-in}^{st-m},B_{ij-in}^{st-m},D_{ij-in}^{st-m}\right)=\int_{h/2}^{h/2+h_{st}}\left(1,z,z^2\right)Q_{ij}^{sti}dz,$$

for $r\in[0,r_0)$.

$$\left(A_{kl-ex}^{st-m},B_{kl-ex}^{st-m},D_{kl-ex}^{st-m}\right)=\int_{h/2}^{h/2+h_{st}}\frac{b_m}{d_m}\left(1,z,z^2\right)Q_{kl}^{ste}dz,$$

$r\in(r_0,R_0]$, for $ij=11,12,22;\ kl=11,22$.

$$\left(A_{22-ex}^{st-p},B_{22-ex}^{st-p},D_{22-ex}^{st-p}\right)=\int_{h/2}^{h/2+h_{st}}\frac{b_p}{d_p}\left(1,z,z^2\right)Q_{kl}^{ste}dz,$$

for $r\in(r_0,R_0]$,

$$\begin{pmatrix}\Phi_{ir}\\ \Phi_{i\theta}\end{pmatrix}=\begin{pmatrix}\Phi_{ir}^{sh}+\Phi_{ir-in}^{st-m}+\Phi_{ir-ex}^{st-m}\\ \Phi_{i\theta}^{sh}+\Phi_{i\theta-in}^{st-m}+\Phi_{i\theta-ex}^{st-p}\end{pmatrix},\ i=1,2,$$

where r_0 is the radius of the concentric region of the radial stiffeners, and

$$\left(\Phi_{1r}^{sh},\Phi_{2r}^{sh}\right)=\int_{-h/2}^{h/2}\left[\left(Q_{11}^{sh}+Q_{12}^{sh}\right)\alpha_{sh}\right](1,z)dz,$$

$$\Phi_{1\theta}^{sh}=\Phi_{1r}^{sh},\Phi_{2\theta}^{sh}=\Phi_{2r}^{sh},$$

$$\left(\Phi_{1r-in}^{st-m},\Phi_{2r-in}^{st-m}\right)=\int_{h/2}^{h/2+h_{st}}\left[\left(Q_{11}^{sti}+Q_{12}^{sti}\right)\alpha_{st}\right](1,z)dz,$$

$$\left(\Phi_{1\theta-in}^{st-m},\Phi_{2\theta-in}^{st-m}\right)=\int_{h/2}^{h/2+h_{st}}\left[\left(Q_{12}^{sti}+Q_{22}^{sti}\right)\alpha_{st}\right](1,z)dz,$$

$r\in[0,r_0)$,

$$\left(\Phi_{1r-ex}^{st-m},\Phi_{2r-ex}^{st-m}\right)=\int_{h/2}^{h/2+h_{st}}\frac{b_m}{d_m}\left(Q_{11}^{ste}\alpha_{st}\right)(1,z)dz,$$

$$\left(\Phi_{1\theta-ex}^{st-p},\Phi_{2\theta-ex}^{st-p}\right)=\int_{h/2}^{h/2+h_{st}}\frac{b_p}{d_p}\left(Q_{22}^{ste}\alpha_{st}\right)(1,z)dz,$$

for $r\in(r_0,R_0]$,

$$Q_{11}^{sh}=Q_{22}^{sh}=\frac{E_{sh}}{1-\nu_{sh}^2},\ Q_{12}^{sh}=\frac{E_{sh}\nu_{sh}}{1-\nu_{sh}^2},$$

$$Q_{11}^{sti}=Q_{22}^{sti}=\frac{E_{st}}{1-\nu_{st}^2},Q_{12}^{sti}=\frac{E_{st}\nu_{st}}{1-\nu_{st}^2},\ \text{for}\ r\in[0,r_0),$$

and $Q_{11}^{ste}=Q_{22}^{ste}=E_{st},\ \text{for}\ r\in(r_0,R_0].$

Conversely, the mid-plane strains ε_{0r} and $\varepsilon_{0\theta}$ are expressed through the extension forces, as

$$\begin{Bmatrix}\varepsilon_{0r}\\ \varepsilon_{0\theta}\end{Bmatrix}=\begin{Bmatrix}A_{11}^* & A_{12}^* & B_{11}^* & B_{12}^*\\ A_{21}^* & A_{22}^* & B_{21}^* & B_{22}^*\end{Bmatrix}\begin{Bmatrix}N_r\\ N_\theta\\ w_{,rr}\\ w_{,r}/r\end{Bmatrix}-\begin{Bmatrix}\Phi_{1r}^*\\ \Phi_{1\theta}^*\end{Bmatrix}\Delta T, \tag{24}$$

where

$$A_{11}^*=\frac{A_{22}}{A_{11}A_{22}-A_{12}^2},A_{12}^*=\frac{-A_{12}}{A_{11}A_{22}-A_{12}^2},$$

$$B_{11}^*=-\frac{(A_{12}B_{12}-A_{22}B_{11})}{A_{11}A_{22}-A_{12}^2},B_{12}^*=-\frac{(A_{12}B_{22}-A_{22}B_{12})}{A_{11}A_{22}-A_{12}^2},$$

$$A_{21}^*=\frac{-A_{12}}{A_{11}A_{22}-A_{12}^2},A_{22}^*=\frac{A_{11}}{A_{11}A_{22}-A_{12}^2},$$

$$B_{21}^*=-\frac{(A_{11}B_{12}-A_{12}B_{11})}{A_{12}^2-A_{11}A_{22}},B_{22}^*=-\frac{(A_{11}B_{22}-A_{12}B_{12})}{A_{12}^2-A_{11}A_{22}},$$

$$\Phi_{1r}^*=\frac{(A_{12}\Phi_{1\theta}-A_{22}\Phi_{1r})}{A_{11}A_{22}-A_{12}^2},\Phi_{1\theta}^*=\frac{(A_{12}\Phi_{1r}-A_{11}\Phi_{1\theta})}{A_{11}A_{22}-A_{12}^2}.$$

Substituting Eq. (24) into Eq. (23), the moment expressions can be rewritten by

$$\begin{Bmatrix}M_r\\ M_\theta\end{Bmatrix}=\begin{Bmatrix}C_{11}^* & C_{12}^* & D_{11}^* & D_{12}^*\\ C_{21}^* & C_{22}^* & D_{21}^* & D_{22}^*\end{Bmatrix}\begin{Bmatrix}N_r\\ N_\theta\\ w_{,rr}\\ w_{,r}/r\end{Bmatrix}-\begin{Bmatrix}\Phi_{2r}^*\\ \Phi_{2\theta}^*\end{Bmatrix}\Delta T. \tag{25}$$

where

$$C_{11}^*=B_{11}A_{11}^*+B_{12}A_{21}^*,C_{12}^*=B_{11}A_{12}^*+B_{12}A_{22}^*,$$

$$D_{11}^*=B_{11}B_{11}^*+B_{12}B_{21}^*-D_{11},C_{21}^*=B_{12}A_{11}^*+B_{22}A_{21}^*,$$

$$D_{12}^*=B_{11}B_{12}^*+B_{12}B_{22}^*-D_{12},C_{22}^*=B_{12}A_{12}^*+B_{22}A_{22}^*,$$

$$D_{21}^*=B_{12}B_{11}^*+B_{22}B_{21}^*-D_{12},$$

$$D_{22}^*=B_{12}B_{12}^*+B_{22}B_{22}^*-D_{22},$$

$$\Phi_{2r}^*=B_{11}\Phi_{1r}^*+B_{12}\Phi_{1\theta}^*+\Phi_{2r},$$

$$\Phi_{2\theta}^*=B_{12}\Phi_{1r}^*+B_{22}\Phi_{1\theta}^*+\Phi_{2\theta},$$

The compatibility equation of spherical shells is established from Eq. (20), as

$$\frac{\varepsilon_{0r,r}}{r}-\varepsilon_{0\theta,rr}-\frac{2\varepsilon_{0\theta,r}}{r}=\frac{1}{R}\left(w_{,r}/r+w_{,rr}\right)+\frac{1}{r}\left(w_{,r}w_{,rr}+w_{,r}w_{0,rr}+w_{,rr}w_{0,r}\right). \tag{26}$$

Introducing the stress function $\varphi(r)$, which satisfies the two following conditions

$$N_r=\frac{\varphi_{,r}}{r},\quad N_\theta=\varphi_{,rr}. \tag{27}$$

The axisymmetric spherical shells are clamped at the circumferential edge, which leads to the following boundary conditions

$$\begin{aligned}&r=0:\ w_{,r}=0,\quad \varphi_{,r}=N_r r=0,\\ &r=R_0:\ w=0,\quad w_{,r}=0,\quad N_r=Q_0,\end{aligned} \tag{28}$$

where Q_0 is the meridian force at the edge, due to the clamped and immovable conditions.

The approximate solution of the deflection, which satisfies boundary condition (28), is chosen as

$$w=\frac{W\left(R_0^2-r^2\right)^2}{R_0^4},\ w_0=\frac{W^*\left(R_0^2-r^2\right)^2}{R_0^4}. \tag{29}$$

where $W^*=\eta h$, with η is the size of the initial imperfection.

Substituting Eq. (27) into Eq. (25), then substituting Eq. (26), the compatibility equation is finally rewritten by taking into account the solution (29), as

$$\begin{aligned}&\frac{\varphi_{,rrr}\left(A_{12}^*-2A_{22}^*-A_{21}^*\right)}{r}-A_{22}^*\varphi_{,rrrr}+\\ &+\frac{\varphi_{,rr}A_{11}^*}{r^2}-\frac{f_{,r}A_{11}^*}{r^3}=\left(\frac{48W^2}{R_0^8}+\frac{96WW^*}{R_0^8}\right)r^4\\ &+\left(\frac{16W^2}{R_0^4}+\frac{32WW^*}{R_0^4}-\frac{8W}{R_0^2R}\right)+72\frac{WB_{21}^*}{R_0^4}\\ &-\left(\frac{64W^2}{R_0^6}+\frac{128WW^*}{R_0^6}-\frac{16W}{R_0^4R}\right)r^2\\ &-24\frac{WB_{11}^*}{R_0^4}+24\frac{WB_{22}^*}{R_0^4}-8\frac{WB_{12}^*}{R_0^4}.\end{aligned} \tag{30}$$

The stress function can be determined using

the coefficient comparison method, as follows

$$\varphi_{,r} = r^7\varphi_7 + r^5\varphi_5 + r^3\varphi_3 + r\varphi_1, \quad (31)$$

where

$$\begin{aligned}\varphi_3 &= X_{31}W^2 + X_{32}WW^* + X_{33}W,\\ \varphi_5 &= X_{51}W^2 + X_{52}WW^* + X_{53}W,\\ \varphi_7 &= X_{71}W^2 + X_{72}WW^*,\end{aligned} \quad (32)$$

with

$$X_{31} = \frac{8}{R_0^4\left[A_{11}^* + 3\left(A_{12}^* - A_{21}^* - 3A_{22}^*\right)\right]},$$

$$X_{32} = \frac{16}{R_0^4\left[A_{11}^* + 3\left(A_{12}^* - A_{21}^* - 3A_{22}^*\right)\right]},$$

$$X_{33} = 4\frac{-3RB_{11}^* - RB_{12}^* + 9RB_{21}^* + 3RB_{22}^* - R_0^2}{RR_0^4\left[A_{11}^* + 3\left(A_{12}^* - A_{21}^* - 3A_{22}^*\right)\right]},$$

$$X_{51} = -16\Big/R_0^6\left[A_{11}^* + 5\left(A_{12}^* - A_{21}^* - 5A_{22}^*\right)\right],$$

$$X_{52} = -32\Big/R_0^6\left[A_{11}^* + 5\left(A_{12}^* - A_{21}^* - 5A_{22}^*\right)\right],$$

$$X_{53} = 4\Big/R_0^4R\left[A_{11}^* + 5\left(A_{12}^* - A_{21}^* - 5A_{22}^*\right)\right],$$

$$X_{71} = \frac{8}{R_0^8\left[A_{11}^* + 7\left(A_{12}^* - A_{21}^* - 7A_{22}^*\right)\right]},$$

$$X_{72} = \frac{16}{R_0^8\left[A_{11}^* + 7\left(A_{12}^* - A_{21}^* - 7A_{22}^*\right)\right]}.$$

The in-plane immovable condition can be expressed in the average sense as

$$\Delta = -\frac{1}{2\pi R_0^2}\int_0^{2\pi}\int_0^{R_0} u_{,r}\,r\,dr\,d\theta = 0. \quad (33)$$

By applying the Eqs. (20), (24), (27), and (28), the condition (33) is obtained by

$$\varphi_1 = X_{11}W^2 + X_{12}WW^* + X_{13}W + X_{14}\Delta T. \quad (34)$$

where

$$X_{11} = \frac{1}{12RR_0^2\left(A_{11}^* + A_{12}^*\right)}\left[\frac{-24RA_{11}^* - 168RA_{12}^*}{A_{11}^* + 7\left(A_{12}^* - A_{21}^* - 7A_{22}^*\right)} + \frac{64RA_{11}^* + 320RA_{12}^*}{A_{11}^* + 5\left(A_{12}^* - A_{21}^* - 5A_{22}^*\right)} - \frac{48RA_{11}^* + 144RA_{12}^*}{A_{11}^* + 3\left(A_{12}^* - A_{21}^* - 3A_{22}^*\right)} + 8R\right],$$

$$X_{12} = \frac{1}{3R_0^2\left(A_{11}^* + A_{12}^*\right)}\left[-\frac{12A_{11}^* + 84A_{12}^*}{A_{11}^* + 7\left(A_{12}^* - A_{21}^* - 7A_{22}^*\right)} + \frac{32A_{11}^* + 160A_{12}^*}{A_{11}^* + 5\left(A_{12}^* - A_{21}^* - 5A_{22}^*\right)} - \frac{24A_{11}^* + 72A_{12}^*}{A_{11}^* + 3\left(A_{12}^* - A_{21}^* - 3A_{22}^*\right)} + 2\right],$$

$$X_{13} = \frac{1}{3RR_0^2\left(A_{11}^* + A_{12}^*\right)}\left[\frac{-4R_0^2\left(A_{11}^* + 5A_{12}^*\right)}{A_{11}^* + 5\left(A_{12}^* - A_{21}^* - 5A_{22}^*\right)} - 6RB_{11}^* + 6RB_{12}^* - R_0^2 - \left(6A_{11}^* + 18A_{12}^*\right)\times \frac{\left(-3RB_{11}^* - RB_{12}^* + 9RB_{21}^* + 3RB_{22}^* - R_0^2\right)}{A_{11}^* + 3\left(A_{12}^* - A_{21}^* - 3A_{22}^*\right)}\right].$$

The total potential energy of the SSpSh is expressed by

$$U_{Total} = U_{int} - U_{ext} \quad (35)$$

where:

$$\begin{aligned}U_{int} &= \pi\int_\Omega\int_0^{r_0}\left[\sigma_r\left(\varepsilon_r - \alpha\Delta T\right) + \sigma_\theta\left(\varepsilon_\theta - \alpha\Delta T\right)\right]r\,dr\,dz\\ &+ \pi\int_\Omega\int_{r_0}^{R_0}\left[\sigma_r\left(\varepsilon_r - \alpha\Delta T\right) + \sigma_\theta\left(\varepsilon_\theta - \alpha\Delta T\right)\right]r\,dr\,dz,\end{aligned} \quad (36)$$

$$\begin{aligned}U_{ext} &= \int_0^{2\pi}\int_{r_0}^{R_0} qwr\,dr\,d\theta\\ &- \frac{1}{2}\int_0^{2\pi}\int_{r_0}^{R_0}\left[\left(K_1w - K_2w_{,rr} - K_2\frac{1}{r}w_{,r}\right)w\right]r\,dr\,d\theta.\end{aligned} \quad (37)$$

where K_1 (N/m^3) and K_2 (N/m) are linear stiffness parameters of the Winkler and Pasternak foundation models, respectively.

Basing the minimum energy principle, i.e.

$$\frac{\partial U_{Total}}{\partial W} = 0. \quad (38)$$

where U_{total} is determined from Eq. (35), leads to

$$\begin{aligned}&a_1WK_2 + a_2WK_1 + a_{31}W^*\Delta T + a_{32}W\Delta T\\ &+a_{33}\Delta T + a_4WW^* + a_{51}W^2W^* + a_{52}WW^*\\ &+a_6W^3 + a_7W^2 + a_8W - \frac{\pi R_0^2q_0}{3} = 0\end{aligned} \quad (39)$$

where a_{ij} is presented in the Appendix.

Eq. (39) explicitly presents the nonlinear dependence among the mechanical load, thermal load, and deflection. Based on this equation, the thermo-mechanical post-buckling responses of stiffened 3D graphene foam SSpShs/CiPls can be easily carried out.

4. Results and discussions

To verify the accuracy of the current solution method, the nonlinear external pressure post-buckling curves of SSpShs are compared with those obtained by Dube et al. [38] for the case of unstiffened isotropic SSpShs (see Fig. 2). The parameter H represent the rise of the SSpSh ($H \approx R_0^2 / 2R$), which reflects the geometric shallowness of the shell. The governing equations in this work are derived based on the FSDT combined with the Galerkin method. The comparison demonstrates strong agreement between the two results. In the numerical examples, the spiderweb-stiffened SSpShs/CiPls composed of 3D graphene foam are examined. The material properties of the GPL and the matrix material are chosen as those in the study by Wang et al. [39].

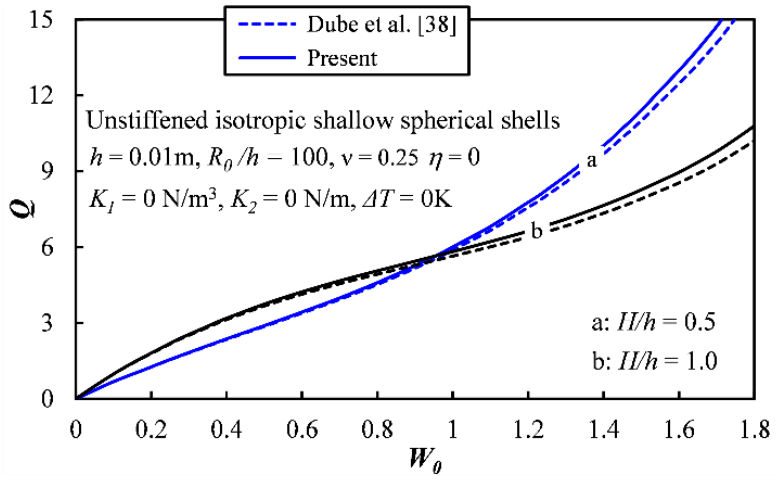

Fig. 2. Comparison of nonlinear external pressure post-buckling curves of SShs, $Q = q_0 R_0^4 / (Eh^4)$

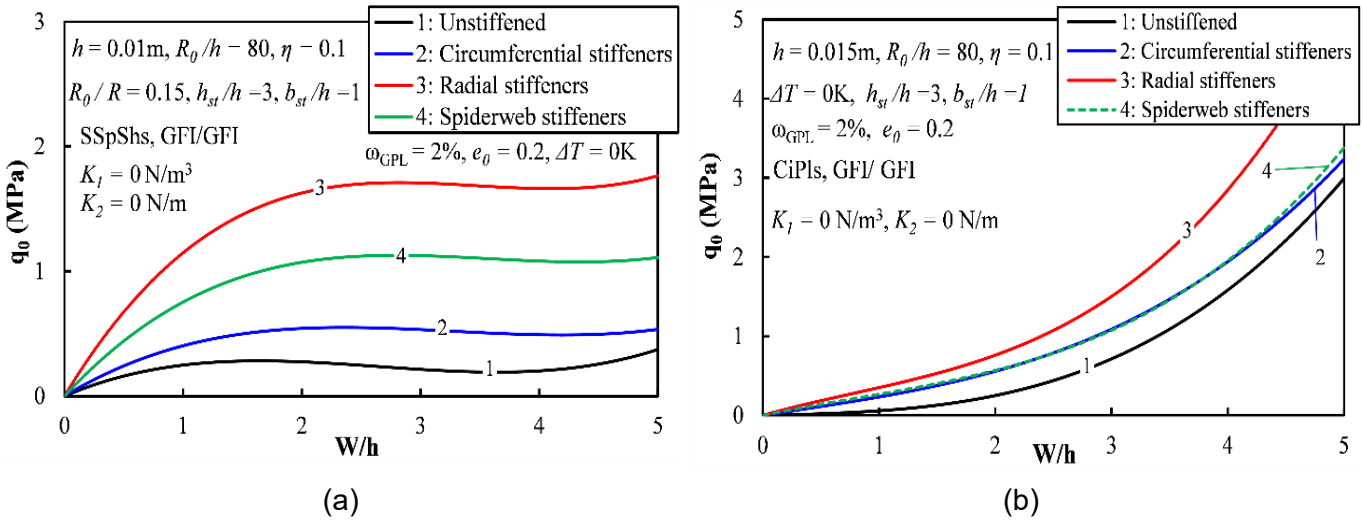

(a) (b)

Fig. 3. Effect of stiffeners on the mechanical and thermal post-buckling responses of 3D graphene foam SSpShs and CiPls

Figs. 3a–d illustrate the mechanical post-buckling curves (3a, 3b) and thermal post-buckling curves (3c, 3d) of SSpShs and CiPls made of 3D graphene foam under the effect of the stiffeners.

Four stiffener configurations were investigated: (1) unstiffened; (2) 10 circumferential stiffeners; (3) 30 radial stiffeners; and (4) a combination of 5 circumferential and 15 radial stiffeners (the "spider web" configuration). In options (2)–(4), the total volume of the stiffeners was adjusted to be nearly the same to ensure a fair comparison. The results show that the presence of stiffeners significantly increases the mechanical and thermal load-bearing capacity. Specifically, for mechanical loading, radial stiffeners are the most effective, followed by the spider web structure. For thermal loading, the load-bearing capacity of the three stiffener configurations is nearly the same. In addition, Fig. 3d indicates that the phenomenon of bifurcation buckling only occurs in the perfect circular plate without stiffeners under thermal loading, whereas it does not appear in any of the stiffened configurations. It can be seen that the stiffeners completely suppress the membrane state, causing deflection to occur immediately upon load application.

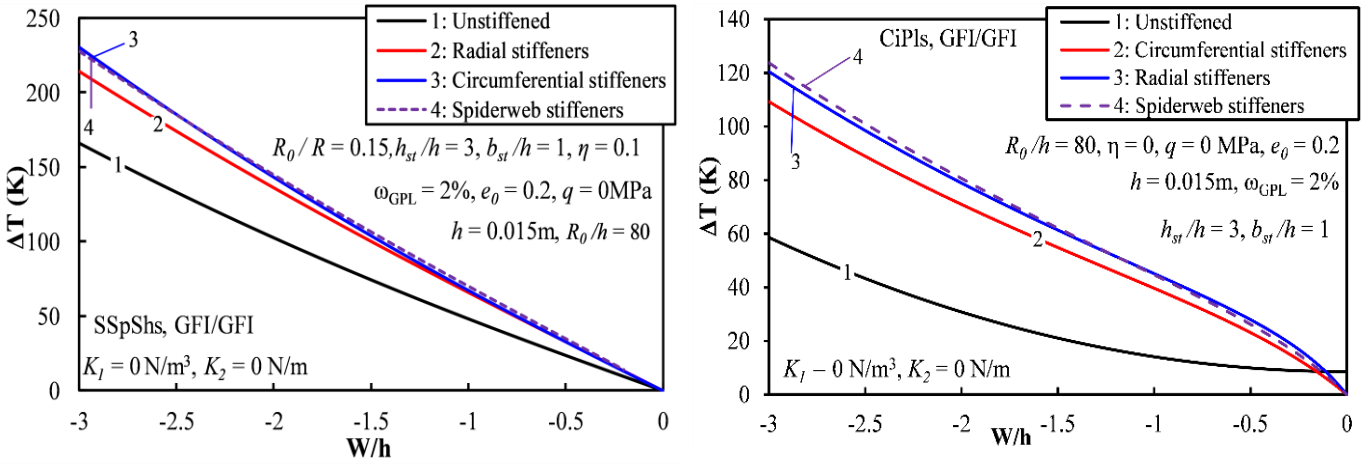

(c) (d)

Fig. 3. (continued)

Fig. 4 considers the effect of the total mass fractions of GPL and the porosity coefficient on the nonlinear mechanical and thermal post-buckling curves of the stiffened SSpShs with different total mass fractions of GPLs (Figs. 4a and 4b) and with different porosity coefficients (Figs. 4c and 4d). It is easy to see in Figs. 4a and 4b that the mechanical and thermal load-carrying capacity of the stiffened SSpShs increases with increasing the total mass fraction of GPLs in the shell and stiffeners. This demonstrates that GPL is an excellent reinforcing material for composite materials to improve mechanical and thermal load-carrying capacity. The effects of the porosity coefficient on the mechanical and thermal post-buckling responses are considered in Figs. 4c and 4d, respectively. As shown in Fig. 4c, the external pressure-carrying capacity of the SSpShs decreases as the porosity coefficient increases. This is expected because a higher porosity coefficient significantly reduces the shell's stiffness, thereby lowering the pressure-carrying capacity of the stiffened SSpShs. In contrast, Fig. 4d indicates that the thermal load-carrying capacity increases with increasing porosity. The opposing effects of decreasing stiffness and increasing thermal expansion exert different influences on the shell behavior, and the results also show that the effect of thermal expansion appears to be dominant.

Figs. 5a and 5b depict the nonlinear mechanical and thermal post-buckling curves of spiderweb-stiffened 3D graphene foam SSpShs with the different material types. Fig. 5a shows that SSpShs with the GFI/GFI distribution law exhibit slightly higher mechanical post-buckling curves compared to the other two distribution laws. This

is because this configuration concentrates more solid material closer to the outer surface, where it contributes more effectively to the bending stiffness. A similar trend is noted for the thermal post-buckling curves in Fig. 5b. However, the difference is very subtle. The nonlinear post-buckling responses of the spiderweb-stiffened 3D graphene foam SSpShs and CiPls with different geometric parameters, such as the R_0/h and R_0/R ratios, are investigated in Figs. 6a-d. These parameters strongly influence the load-bearing capacity of stiffened 3D graphene foam SSpShs and CiPls. Figs. 6a and 6b illustrate how the R_0/h ratio affects the post-buckling response of stiffened 3D graphene foam SSpShs and CiPls under mechanical or thermal loading. It is observed that the R_0/h ratio has a more pronounced influence on the mechanical and thermal post-buckling responses of stiffened 3D graphene foam SSpShs and CiPls compared with their unstiffened structures. Fig. 6a also indicates that the spiderweb stiffener system markedly decreases the snap-through intensity of SSpShs, particularly in thin structures. The influence of the R_0/R ratio on the nonlinear post-buckling curves of stiffened 3D graphene foam SSpShs and CiPls is clearly reflected in Figs. 6c and 6d. The results indicate that the maximum post-buckling load (represented by these curves) increases as the R_0/R ratio increases, which corresponds to a decrease in the shallowness of the SSpShs.

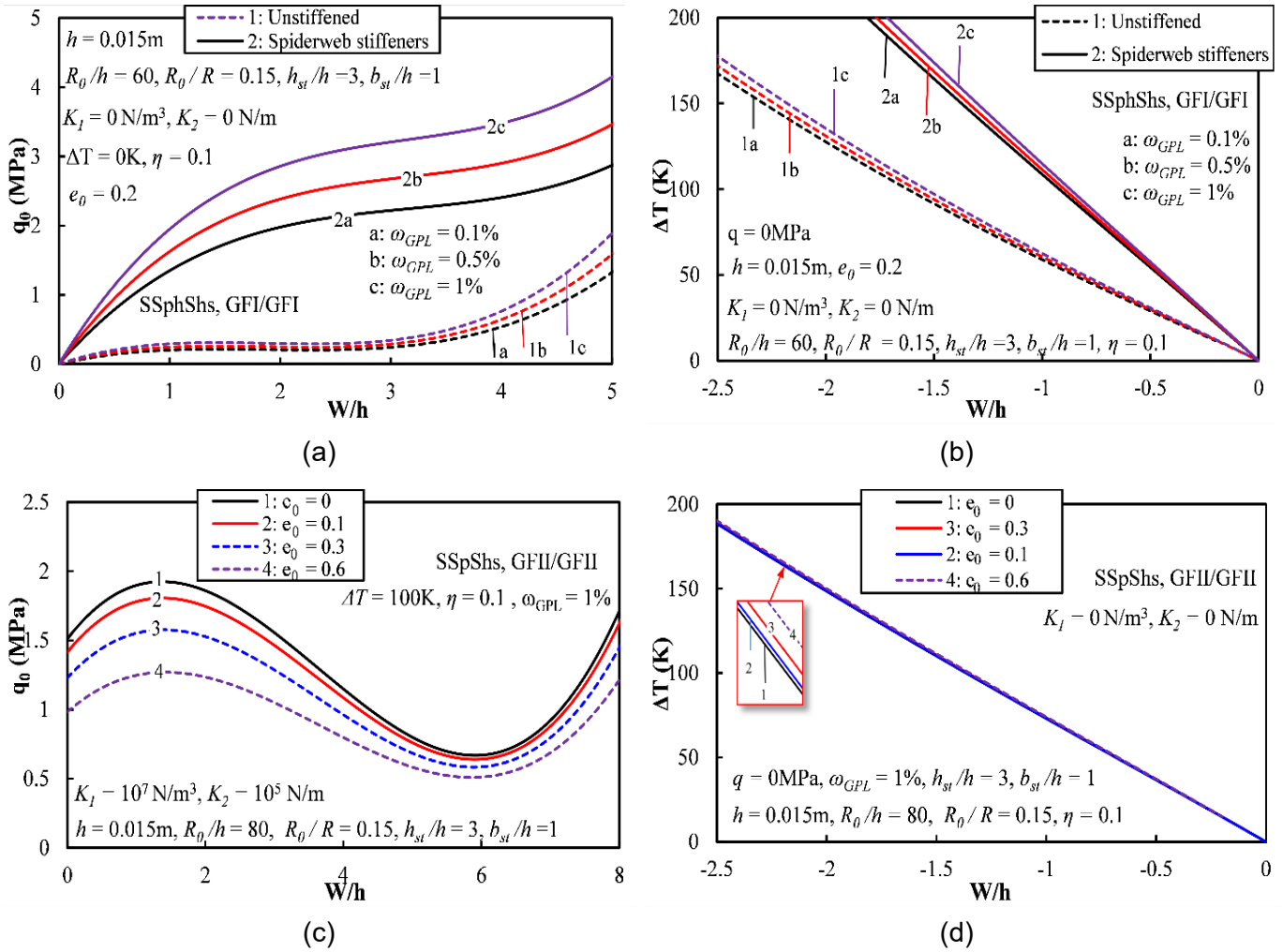

Fig. 4. Effect of total mass fractions of GPLs and porosity coefficient on the mechanical and thermal post-buckling responses of spiderweb-stiffened 3D graphene foam SSpShs.

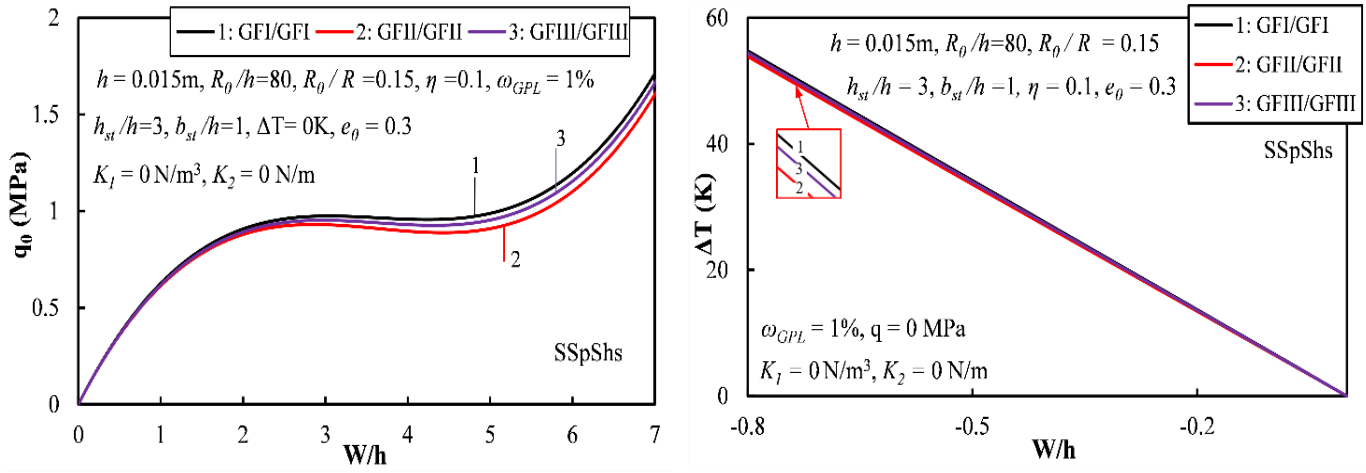

(a) (b)

Fig. 5. Mechanical and thermal post-buckling responses of spiderweb-stiffened 3D graphene foam SSpShs with the different material types.

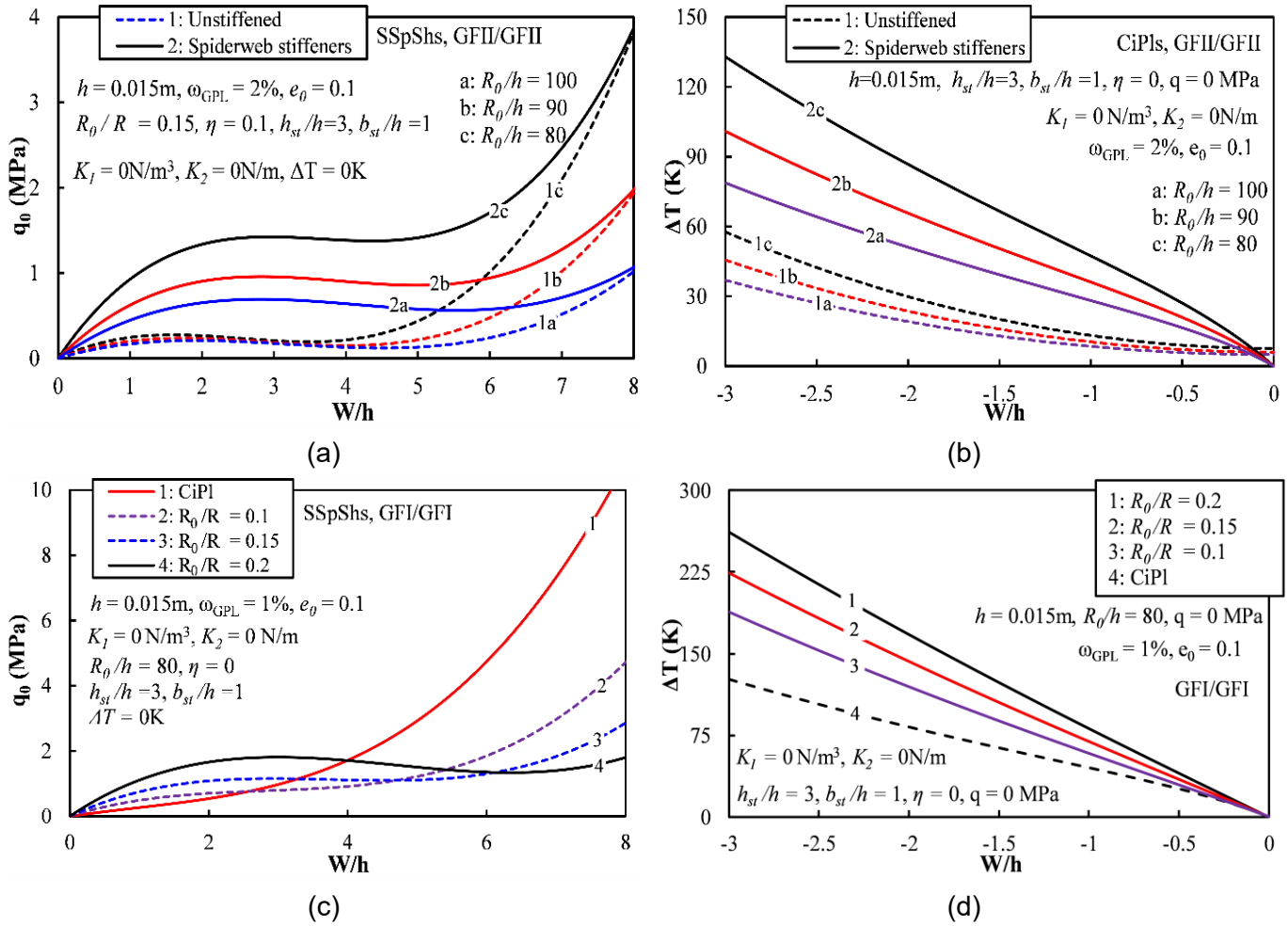

(a) (b)

(c) (d)

Fig. 6. Effect of geometric parameters on the mechanical and thermal post-buckling responses of spiderweb-stiffened 3D graphene foam SSpShs and CiPls

5. Conclusion

This paper presented an analytical framework for the thermo-mechanical post-buckling analysis of 3D graphene foam SSpShs and CiPls stiffened by a spider-web stiffener system, using a stress function formulation. The

proposed model accounts for geometric nonlinearity, and the combined effect of radial and circumferential stiffeners through an extended smeared-stiffener approach. By applying the Ritz energy minimization method, the load-deflection post-buckling relations are derived. The numerical results examine how geometric parameters, material properties, and spiderweb stiffeners influence the nonlinear mechanical and thermal post-buckling responses of stiffened 3D graphene foam SSpShs and CiPls. The key findings can be summarized as follows

- In all cases examined, stiffened 3D graphene foam SSpShs and CiPls show a markedly higher post-buckling load-carrying capacity than their unstiffened structures. For the input data considered, SSpShs/CiPls stiffened by radial stiffeners exhibit the highest load-carrying capacity. Meanwhile, the thermal load-carrying capacity of the plate/shell with different reinforcement options shows little difference.

- Among all cases examined, SSpShs with the GFI/GFI material distribution show the highest mechanical and thermal load-carrying capacity, whereas those with the GFII/GFII type show the lowest. However, the difference is negligible.

- The nonlinear post-buckling curves of spiderweb- stiffened 3D graphene foam SSpShs and CiPls are strongly influenced by the stiffeners, and R_0 / h and R_0 / R ratios.

Declaration of conflicting interests: The author(s) declared no potential conflicts of interest with respect to the research, authorship, and/or publication of this article.

Acknowledgments: This research is funded by Vietnam National Foundation for Science and Technology Development (NAFOSTED) under grant number 107.02-2023.45.

References

[1] B. Pan, W. Cui. (2010). An overview of buckling and ultimate strength of spherical pressure hull under external pressure. *Marine Structures*, 23(3), 227–240. https://doi.org/10.1016/j.marstruc.2010.07.005

[2] T.Y. Wu, G.R. Liu. (2001). Free vibration analysis of circular plates with variable thickness by the generalized differential quadrature rule. *International Journal of Solids and Structures*, 38(44), 7967–7980. https://doi.org/10.1016/S0020-7683(01)00077-4

[3] R. Shahsiah, M.R. Eslami. (2003). Thermal and Mechanical Instability of an Imperfect Shallow Spherical Cap. *Journal of Thermal Stresses*, 26(7), 723–737. https://doi.org/10.1080/713855992

[4] A. Kalnins, P.M. Naghdi. (1960). Axisymmetric Vibrations of Shallow Elastic Spherical Shells. *The Journal of the Acoustical Society of America*, 32(3), 342–347. https://doi.org/10.1121/1.1908055

[5] P.L. Grossman, B. Koplik, Y.-Y. Yu. (1969). Nonlinear Vibrations of Shallow Spherical Shells. *Journal of Applied Mechanics*, 36(3), 451–458. https://doi.org/10.1115/1.3564701

[6] M. Sathyamoorthy. (1994). Vibrations of Moderately Thick Shallow Spherical Shells at Large Amplitudes. *Journal of Sound and Vibration*, 172(1), 63–70. https://doi.org/10.1006/jsvi.1994.1158

[7] H. Abels, H. Garcke, L. Müller. (2015). Stability of spherical caps under the volume-preserving mean curvature flow with line tension. *Nonlinear Analysis: Theory, Methods & Applications*, 117, 8–37. https://doi.org/10.1016/j.na.2014.11.020

[8] A. Li, X. Ji, S. Zhou, L. Wang, J. Chen, P. Liu. (2021). Nonlinear axisymmetric bending analysis of strain gradient thin circular plate. *Applied Mathematical Modelling*, 89, 363–380. https://doi.org/10.1016/j.apm.2020.08.004

[9] M. Najafipour, M. Shariyat. (2023). A refined first-order shear deformation theory for large dynamic and static deflection investigations of abruptly/harmonically pressurized/blasted incompressible circular hyperelastic plates.

Ocean Engineering, 289, 116185. https://doi.org/10.1016/j.oceaneng.2023.116185

[10] Y. Kiani. (2017). Axisymmetric static and dynamics snap-through phenomena in a thermally postbuckled temperature-dependent FGM circular plate. *International Journal of Non-Linear Mechanics*, 89, 1–13. https://doi.org/10.1016/j.ijnonlinmec.2016.11.003

[11] H. Ahmadi, K. Foroutan. (2021). Nonlinear buckling analysis of FGP shallow spherical shells under thermomechanical condition. *Steel and Composite Structures*, 40(4), 555–570. https://doi.org/10.12989/scs.2021.40.4.555

[12] Y. Fu, S. Hu, Y. Mao. (2014). Nonlinear transient response of functionally graded shallow spherical shells subjected to mechanical load and unsteady temperature field. *Acta Mechanica Solida Sinica*, 27(5), 496–508. https://doi.org/10.1016/S0894-9166(14)60058-6

[13] V.T.T. Anh, N.D. Duc. (2016). Nonlinear response of a shear deformable S-FGM shallow spherical shell with ceramic-metal-ceramic layers resting on an elastic foundation in a thermal environment. *Mechanics of Advanced Materials and Structures*, 23(8), 926–934. https://doi.org/10.1080/15376494.2015.1059527

[14] N.T. Phuong, V.H. Nam, D.T. Dong. (2020). Nonlinear vibration of functionally graded sandwich shallow spherical caps resting on elastic foundations by using first-order shear deformation theory in thermal environment. *Journal of Sandwich Structures & Materials*, 22(4), 1157–1183. https://doi.org/10.1177/1099636218782645

[15] H. Zhou, K. Han, L. Elmaimouni, X. Wang, J. Yu. (2024). Double Legendre polynomial quadrature-free method for axisymmetric vibration of functionally graded piezoelectric circular plates. *Journal of Vibration and Control*, 30(3-4), 598–615. https://doi.org/10.1177/10775463221149087

[16] N.L. Le, T.N.T. Duong, T.D. Dang, M.D. Vu, T.T. Bui, T.P. Nguyen, H.N. Vu. (2023). A Novel Analytical Approach for Nonlinear Thermo-Mechanical Buckling of Higher-Order Shear Deformable Porous Circular Plates and Spherical Caps with FGM Face Sheets. *International Journal of Applied Mechanics*, 15(05), 2350035. https://doi.org/10.1142/S1758825123500357

[17] M. Javani, Y. Kiani, M.R. Eslami. (2024). Nonlinear dynamic response of a temperature-dependent FGM spherical shell under various boundary conditions and thermal shocks: Examination of dynamic snap-through. *Thin-Walled Structures*, 199, 111796. https://doi.org/10.1016/j.tws.2024.111796

[18] C.H. Thai, P.P.-Van. (2020). A meshfree approach using naturally stabilized nodal integration for multilayer FG GPLRC complicated plate structures. *Engineering Analysis with Boundary Elements*, 117, 346–358. https://doi.org/10.1016/j.enganabound.2020.04.001

[19] D. Liu, Y. Zhou, J. Zhu. (2021). On the free vibration and bending analysis of functionally graded nanocomposite spherical shells reinforced with graphene nanoplatelets: Three-dimensional elasticity solutions. *Engineering Structures*, 226, 111376. https://doi.org/10.1016/j.engstruct.2020.111376

[20] C. Chu, M.S.H. Al-Furjan, R. Kolahchi, A. Farrokhian. (2023). A nonlinear Chebyshev-based collocation technique to frequency analysis of thermally pre/post-buckled third-order circular sandwich plates. *Communications in Nonlinear Science and Numerical Simulation*, 118, 107056. https://doi.org/10.1016/j.cnsns.2022.107056

[21] M. Javani, Y. Kiani, M.R. Eslami. (2021). Geometrically nonlinear free vibration of FG-

GPLRC circular plate on the nonlinear elastic foundation. *Composite Structures*, 261, 113515. https://doi.org/10.1016/j.compstruct.2020.113515

[22] T.T. Bui, M.D. Vu, N.N. Pham, V.D. Cao, H.N. Vu. (2024). Nonlinear thermo-mechanical dynamic buckling and vibration of FG-GPLRC circular plates and shallow spherical shells resting on the nonlinear viscoelastic foundation. *Archive of Applied Mechanics*, 94(12), 3715–3729. https://doi.org/10.1007/s00419-024-02691-6

[23] T.P. Nguyen, T.D. Dang, T.T. Bui, M.D. Vu, K. Le-Nguyen, T.H. Pham, H.N. Vu. (2024). Nonlinear thermo-mechanical axisymmetric stability of FG-GPLRC spherical shells and circular plates resting on nonlinear elastic medium. *Ships and Offshore Structures*, 19(6), 820–830. https://doi.org/10.1080/17445302.2023.2214489

[24] N.L. Le, T.T. Bui, T.N.T. Duong, T.D. Dang, M.D. Vu, T.P. Nguyen. (2023). Nonlinear thermo-mechanical buckling and postbuckling of sandwich FG-GPLRC spherical caps and circular plates with porous core by using higher-order shear deformation theory. *Journal of Thermoplastic Composite Materials*, 36(10), 4083–4105. https://doi.org/10.1177/08927057221147827

[25] A. Idowu, B. Boesl, A. Agarwal. (2018). 3D graphene foam-reinforced polymer composites – A review. *Carbon*, 135, 52–71. https://doi.org/10.1016/j.carbon.2018.04.024

[26] W. Peng, H.L. Ferrand. (2025). Mechanical properties of template-based 3D graphene foams via multiscale modeling. *International Journal of Mechanical Sciences*, 303, 110621. https://doi.org/10.1016/j.ijmecsci.2025.110621

[27] M. Khatounabadi, M. Jafari, K. Asemi. (2025). Low-velocity impact analysis of functionally graded porous circular plate reinforced with graphene platelets. *Waves in Random and Complex Media*, 35(4), 7838–7864. https://doi.org/10.1080/17455030.2022.2091182

[28] B.T. Tu, N.T. Phuong, L.N. Ly, V.T. Hung, V.H. Nam. (2025). A New Analytical Approach to the Nonlinear Thermo-Mechanical Buckling Behavior of Three-Dimensional Graphene Foams-Reinforced Complexly Curved Caps and Circular Plates. *International Journal of Structural Stability and Dynamics*, 25(16), 2550169. https://doi.org/10.1142/S021945542550169X

[29] S.G. Lekhnitskii. (1968). Anisotropic Plates. *Gordon and Breach Science Publishers*. *New York.*

[30] N. Jaunky, N.F. Knight, D.R. Ambur. (1996). Formulation of an improved smeared stiffener theory for buckling analysis of grid-stiffened composite panels. *Composites Part B: Engineering*, 27(5), 519–526. https://doi.org/10.1016/1359-8368(96)00032-7

[31] M.M. Najafizadeh, A. Hasani, P. Khazaeinejad. (2009). Mechanical stability of functionally graded stiffened cylindrical shells. *Applied Mathematical Modelling*, 33(2), 1151–1157. https://doi.org/10.1016/j.apm.2008.01.009

[32] D.H. Bich, D.V. Dung, V.H. Nam. (2012). Nonlinear dynamical analysis of eccentrically stiffened functionally graded cylindrical panels. *Composite Structures*, 94(8), 2465–2473. https://doi.org/10.1016/j.compstruct.2012.03.012

[33] V.H. Nam, D.T. Dong, C.V. Doan, N.T. Phuong. (2022). Nonlinear Thermo-Electro-Mechanical Buckling of Higher-Order Shear Deformable Stiffened FG-GRC Laminated Plates. *International Journal of Applied Mechanics*, 14(06), 2250051. https://doi.org/10.1142/S175882512250051X

[34] V.H. Nam, D.T. Dong, C. Van Doan, N.T. Phuong. (2022). Nonlinear buckling of axially compressed FG-GRCL stiffened cylindrical panels with a piezoelectric layer by using Reddy's higher-order shear deformation theory.

Polymer Composites, 43(11), 7952–7966. https://doi.org/10.1002/pc.26931

[35] H.N. Vu, T.P. Nguyen, S.L. Ho, M.D. Vu, V.D. Cao. (2023). Nonlinear buckling analysis of stiffened FG-GRC laminated cylindrical shells subjected to axial compressive load in thermal environment. *Mechanics Based Design of Structures and Machines*, 51(7), 3678–3694. https://doi.org/10.1080/15397734.2021.1932522

[36] V.H. Nam, T.Q. Minh, P.T. Hieu, V.T. Hung, B.T. Tu, N.T.T. Hoai, D.T. Dong. (2023). A new analytical approach for nonlinear thermo-mechanical postbuckling of FG-GPLRC circular plates and shallow spherical caps stiffened by spiderweb stiffeners. *Thin-Walled Structures*, 193, 111296. https://doi.org/10.1016/j.tws.2023.111296

[37] J. Yang, D. Chen, S. Kitipornchai. (2018). Buckling and free vibration analyses of functionally graded graphene reinforced porous nanocomposite plates based on Chebyshev-Ritz method. *Composite Structures*, 193, 281–294.https://doi.org/10.1016/j.compstruct.2018.03.090

[38] G.P. Dube, S. Joshi, P.C. Dumir. (2001). Nonlinear analysis of thick shallow spherical and conical orthotropic caps using Galerkin's method. *Applied Mathematical Modelling*, 25(9), 755–773. https://doi.org/10.1016/S0307-904X(01)00012-9

[39] Y. Wang, Y. Kiani. (2022). Effects of initial compression/tension, foundation damping and pasternak medium on the dynamics of shear and normal deformable GPLRC beams under moving load. *Materials Today Communications*, 33, 104938. https://doi.org/10.1016/j.mtcomm.2022.104938

Appendix

a_{ij} are determined as follows

$$a_1 = \int_0^{R_0} -2\frac{\pi\left(R_0^{\,2} - r^2\right)^2 r}{R_0^{\,4}}\left(8\frac{r^2}{R_0^{\,4}} - 8\frac{R_0^{\,2} - r^2}{R_0^{\,4}}\right)dr,\ a_2 = \int_0^{R_0} 2\frac{\pi\left(R_0^{\,2} - r^2\right)^4 r}{R_0^{\,8}}dr$$

$$a_{31} = \int_0^{R_0}\begin{pmatrix} N_{rg2-r}\left(X_{14}A_{11}^* + X_{14}A_{12}^* - \Phi_{1r}^*\right) + X_{14}\left(A_{11}^* N_{rg2-r} + A_{12}^* N_{\theta g2-r}\right) + N_{\theta g2-r}\left(X_{14}A_{21}^* + X_{14}A_{22}^* - \Phi_{1\theta}^*\right) \\ +X_{14}\left(A_{21}^* N_{rg2-r} + A_{22}^* N_{\theta g2-r}\right) - \left(\Phi_{1r}\left(A_{11}^* N_{rg2-r} + A_{12}^* N_{\theta g2-r}\right) + \Phi_{1\theta}\left(A_{21}^* N_{rg2-r} + A_{22}^* N_{\theta g2-r}\right)\right) \end{pmatrix} r\pi dr$$

$$a_{32} = \int_0^{R_0}\begin{pmatrix} 2N_{rg1-r}\left(X_{14}A_{11}^* + X_{14}A_{12}^* - \Phi_{1r}^*\right) + X_{14}\left(2A_{11}^* N_{rg1-r} + 2A_{12}^* N_{\theta g1-r}\right) + 2N_{\theta g1-r}\left(X_{14}A_{21}^* + X_{14}A_{22}^* - \Phi_{1\theta}^*\right) \\ +X_{14}\left(2A_{21}^* N_{rg1-r} + 2A_{22}^* N_{\theta g1-r}\right) - \left(\Phi_{1r}\left(2A_{11}^* N_{rg1-r} + 2A_{12}^* N_{\theta g1-r}\right) + \Phi_{1\theta}\left(2A_{21}^* N_{rg1-r} + 2A_{22}^* N_{\theta g1-r}\right)\right) \end{pmatrix} r\pi dr$$

$$a_4 = \int_0^{R_0}\left(2N_{rg2-r}\left(A_{11}^* N_{rg2-r} + A_{12}^* N_{\theta g2-r}\right) + 2N_{\theta g2-r}\left(A_{21}^* N_{rg2-r} + A_{22}^* N_{\theta g2-r}\right)\right) r\pi dr,$$

$$a_{33} = \int_0^{R_0}\begin{pmatrix} +N_{rg3-r}\left(X_{14}A_{11}^* + X_{14}A_{12}^* - \Phi_{1r}^*\right) + X_{14}\left(N_{rg3-r}A_{11}^* + \lambda B_{11}^* - 4\delta B_{12}^* + A_{12}^* N_{\theta g3-r}\right) \\ +4\delta\left(X_{14}C_{21}^* + Y_{14}C_{22}^* - \Phi_{2\theta}^*\right) + N_{\theta g3-r}\left(X_{14}A_{21}^* + Y_{14}A_{22}^* - \Phi_{1\theta}^*\right) \\ +X_{14}\left(N_{rg3-r}A_{21}^* + \lambda B_{21}^* - 4\delta B_{22}^* + A_{22}^* N_{\theta g3-r}\right) - \left(X_{14}C_{11}^* + Y_{14}C_{12}^* - \Phi_{2r}^*\right)\lambda \end{pmatrix} r\pi$$
$$-\begin{pmatrix} \Phi_{1r}\left(N_{rg3-r}A_{11}^* + \lambda B_{11}^* - 4\delta B_{12}^* + A_{12}^* N_{\theta g3-r}\right) - \Phi_{2r}\lambda \\ +\Phi_{1\theta}\left(N_{rg3-r}A_{21}^* + \lambda B_{21}^* - 4\delta B_{22}^* + A_{22}^* N_{\theta g3-r}\right) + 4\Phi_{2\theta}\delta \end{pmatrix} r\pi dr,$$

$$a_{51} = \int_0^{R_0}\begin{pmatrix} N_{rg2\text{-}r}\left(A_{11}^* N_{rg1\text{-}r} + A_{12}^* N_{\theta g1\text{-}r}\right) + 3N_{rg1\text{-}r}\left(A_{11}^* N_{rg2\text{-}r} + A_{12}^* N_{\theta g2\text{-}r}\right) + N_{rg2\text{-}r}\left(2A_{11}^* N_{rg1\text{-}r} + 2A_{12}^* N_{\theta g1\text{-}r}\right) \\ +N_{\theta g2\text{-}r}\left(A_{21}^* N_{rg1\text{-}r} + A_{22}^* N_{\theta g1\text{-}r}\right) + 3N_{\theta g1\text{-}r}\left(A_{21}^* N_{rg2\text{-}r} + A_{22}^* N_{\theta g2\text{-}r}\right) + N_{\theta g2\text{-}r}\left(2A_{21}^* N_{rg1\text{-}r} + 2A_{22}^* N_{\theta g1\text{-}r}\right) \end{pmatrix} r\pi dr,$$

$$a_{52} = \int_0^{R_0}\begin{pmatrix} +2N_{rg3\text{-}r}\left(A_{11}^* N_{rg2\text{-}r} + A_{12}^* N_{\theta g2\text{-}r}\right) + 2N_{rg2\text{-}r}\left(N_{rg3\text{-}r}A_{11}^* + \lambda B_{11}^* - 4\delta B_{12}^* + A_{12}^* N_{\theta g3\text{-}r}\right) \\ +8\delta\left(C_{21}^* N_{rg2\text{-}r} + C_{22}^* N_{\theta g2\text{-}r}\right) + 2N_{\theta g3\text{-}r}\left(A_{21}^* N_{rg2\text{-}r} + A_{22}^* N_{\theta g2\text{-}r}\right) \\ +2N_{\theta g2\text{-}r}\left(N_{rg3\text{-}r}A_{21}^* + \lambda B_{21}^* - 4\delta B_{22}^* + A_{22}^* N_{\theta g3\text{-}r}\right) - 2\left(C_{11}^* N_{rg2\text{-}r} + C_{12}^* N_{\theta g2\text{-}r}\right)\lambda \end{pmatrix} r\pi dr,$$

$$a_6 = \int_0^{R_0}\begin{pmatrix} 2N_{rg1\text{-}r}\left(A_{11}^* N_{rg1\text{-}r} + A_{12}^* N_{\theta g1\text{-}r}\right) + N_{rg1\text{-}r}\left(2A_{11}^* N_{rg1\text{-}r} + 2A_{12}^* N_{\theta g1\text{-}r}\right) \\ +2N_{\theta g1\text{-}r}\left(A_{21}^* N_{rg1\text{-}r} + A_{22}^* N_{\theta g1\text{-}r}\right) + N_{\theta g1\text{-}r}\left(2A_{21}^* N_{rg1\text{-}r} + 2A_{22}^* N_{\theta g1\text{-}r}\right) \end{pmatrix} r\pi dr,$$

$$a_7 = \int_0^{R_0}\begin{pmatrix} -\left(2C_{11}^* N_{rg1\text{-}r} + 2C_{12}^* N_{\theta g1\text{-}r}\right)\lambda - \left(C_{11}^* N_{rg1\text{-}r} + C_{12}^* N_{\theta g1\text{-}r}\right)\lambda + N_{rg3\text{-}r}\left(A_{11}^* N_{rg1\text{-}r} + A_{12}^* N_{\theta g1\text{-}r}\right) \\ +N_{rg3\text{-}r}\left(2A_{11}^* N_{rg1\text{-}r} + 2A_{12}^* N_{\theta g1\text{-}r}\right) + 4\delta\left(C_{21}^* N_{rg1\text{-}r} + C_{22}^* N_{\theta g1\text{-}r}\right) + N_{\theta g3\text{-}r}\left(2A_{21}^* N_{rg1\text{-}r} + 2A_{22}^* N_{\theta g1\text{-}r}\right) \\ +3N_{rg1\text{-}r}\left(N_{rg3\text{-}r}A_{11}^* + \lambda B_{11}^* - 4\delta B_{12}^* + A_{12}^* N_{\theta g3\text{-}r}\right) + 4\delta\left(2C_{21}^* N_{rg1\text{-}r} + 2C_{22}^* N_{\theta g1\text{-}r}\right) \\ +N_{\theta g3\text{-}r}\left(A_{21}^* N_{rg1\text{-}r} + A_{22}^* N_{\theta g1\text{-}r}\right) + 3N_{\theta g1\text{-}r}\left(N_{rg3\text{-}r}A_{21}^* + \lambda B_{21}^* - 4\delta B_{22}^* + A_{22}^* N_{\theta g3\text{-}r}\right) \end{pmatrix} r\pi dr,$$

$$a_8 = \int_0^{R_0}\begin{pmatrix} -2\left(N_{rg3\text{-}r}C_{11}^* + \lambda D_{11}^* - 4\delta D_{12}^* + C_{12}^* N_{\theta g3\text{-}r}\right)\lambda + 2N_{rg3\text{-}r}\left(N_{rg3\text{-}r}A_{11}^* + \lambda B_{11}^* - 4\delta B_{12}^* + A_{12}^* N_{\theta g3\text{-}r}\right) \\ +8\delta\left(N_{rg3\text{-}r}C_{21}^* + \lambda D_{21}^* - 4\delta D_{22}^* + C_{22}^* N_{\theta g3\text{-}r}\right) + 2N_{\theta g3\text{-}r}\left(N_{rg3\text{-}r}A_{21}^* + \lambda B_{21}^* - 4\delta B_{22}^* + A_{22}^* N_{\theta g3\text{-}r}\right) \end{pmatrix} r\pi dr,$$

where

$N_{rg1-r} = X_{71}r^6 + X_{51}r^4 + X_{31}r^2 + X_{11}, N_{rg2-r} = X_{72}r^6 + X_{52}r^4 + X_{32}r^2 + X_{12}$,

$\lambda = \left(8\frac{r^2}{R_0^{\,4}} - 4\frac{R_0^{\,2} - r^2}{R_0^{\,4}} \right), \delta = \frac{(R_0^{\,2} - r^2)}{R_0^{\,4}}$, $N_{rg3-r} = X_{53}r^4 + X_{33}r^2 + X_{13}, N_{\theta g1-r} = 7X_{71}r^6 + 5X_{51}r^4 + 3X_{31}r^2 + X_{11},$

$N_{\theta g2-r} = 7X_{72}r^6 + 5X_{52}r^4 + 3X_{32}r^2 + X_{12}, N_{\theta g3-r} = 5X_{53}r^4 + 3X_{33}r^2 + X_{13}$